Wind and Structures, *Vol. 18, No. 3 (2014) 295-320*
DOI: http://dx.doi.org/10.12989/was.2014.18.3.295

Power spectra of wind forces on a high-rise building with section varying along height

D.M. Huang[*1,2,3], L.D. Zhu[2] and W. Chen[2]

[1]*School of Civil Engineering, Central South University, Changsha 410075, China*
[2]*State Key Laboratory for Disaster Reduction in Civil Engineering, Tongji University, Shanghai 200092, China*
[3]*National Engineering Laboratory for High Speed Railway Construction, Central South University, Changsha 410075, China*

(Received July 12, 2012, Revised November 17, 2013, Accepted December 27, 2013)

Abstract. The characteristics of amplitudes and power spectra of X axial, Y axial, and RZ axial (i.e., body axis) wind forces on a 492 m high-rise building with a section varying along height in typical wind directions are studied via a rigid model wind tunnel test of pressure measurement. Then the corresponding mathematical expressions of power spectra of X axial (across-wind), Y axial (along-wind) and torsional wind forces in 315^{o} wind directions are proposed. The investigation shows that the mathematical expressions of wind force spectra of the main structure in across-wind and torsional directions can be constructed by the superimposition of an modified wind spectrum function and a peak function caused by turbulent flow and vortex shedding, respectively. While that in along-wind direction can only be constructed by the former and is similar to wind spectrum. Moreover, the fitted parameters of the wind load spectra of each measurement level of altitude are summarized, and the unified parametric results are obtained. The comparisons of the first three order generalized force spectra show that the proposed mathematical expressions accord with the experimental results well.

Keywords: high-rise building; rigid model wind tunnel test of pressure measurement; wind force spectrum; mathematical expressions; parameters fitting

1. Introduction

Numerous skyscrapers have been constructed with the development of modern materials and construction technique. The wind load becomes the critical factor on structural safety and serviceability with the increase of height and flexibility of these numerous skyscrapers.

In the early stages, quasi-steady theory was used to determine the wind loads in along-wind direction due to the limitation of test conditions as the atmospheric boundary layer wind tunnel (Simiu and Scanlan 1986, Davenport 1961, 1967), which means that the power spectra and coherence functions of wind loads on structure were derived from that of approaching flow wind speed. However, since the civil engineering structures are generally bluff bodies with irregular cross-section , which would induce irregular flow and vortex shedding phenomena, the quasi-steady theory become inaccurate in deriving along-wind loads and unavailable in

*Corresponding author, Associate professor, E-mail: huangdongmei_tumu@163.com

http://www.techno-press.org/?journal=was&subpage=8 ISSN: 1226-6116 (Print), 1598-6225 (Online)

determining cross-wind and torsional loads. Recently, with the development of wind tunnel test techniques such as aeroelastic model test technique, high-frequency dynamic balance test technique and synchronous multi-pressure measurement test technique, the detailed characteristics and mathematical models of unsteady wind load spectra have been investigated, not only in along-wind but also in cross-wind and torsional directions.

The researches on wind load spectra based on single degree of freedom aeroelastic model test were in the 1970s and 1980s.Saunders and Melbourne (1975) studied the influences of aspect ratio, size ratio, turbulence intensity and reduced wind speed on the cross-wind aerodynamic force spectra of square and rectangular buildings, and then drawn the following conclusions: 1. the aerodynamic force and response of cross-wind were caused by the wake flow; 2. the band of aerodynamics force spectrum widened significantly with turbulence intensity increasing; 3. the band of aerodynamics force spectrum became narrower with the ratio of across-wind width to along-wind width reducing; 4. the vibration amplitude of a structure had little influence on the reduced cross-wind force spectrum. Afterward, Kwok (1982, 1995) investigated the cross-wind force spectra of circular and square cross-section columns. They found that the generalized aerodynamic force spectrum significantly increased because of the lock-in action when the reduced wind speed corresponding to spectrum-peak approached to vortex-induced resonance wind speed. It amended the 4th conclusion of Saunders and Melbourne (1975). After 1980s, the high-frequency dynamic balance model test and the synchronous multi-pressure measurement test became the mainly methods for investigating wind load power spectra.

The generalized wind force spectrum could be obtained easily via the high-frequency dynamic balance model test. Kareem (1992) investigated the generalized aerodynamic spectra in along-wind, cross-wind, and torsion directions of high-rise buildings with different shapes under two kinds of wind fields and gave the procedure for calculating responses. Marukawa *et al*. (1992) researched the features of the generalized cross-wind and torsion aerodynamic force spectra of a series of rectangular cross-section tall buildings with different height-width ratios, length-width ratios and in different wind fields. A mathematical model for generalized across-wind force spectrum was then presented, which was cited by Architectural Institute of Japan (1996). Gu and Quan (2004) put forward a comprehensive mathematical model for generalized across-wind aerodynamic spectrum of tall buildings, which could consider different types of wind fields, aspect ratios, and size ratios.

The technique of high-frequency dynamic balance model test can obtain the base moment and then the equivalent static loads on each floor by assuming the mode shape linear (Zhou *et al*. 1999a, b).However, it is unavailable for the spatial distribution of wind pressure and thus the power spectra of local wind forces. Therefore, the synchronous multi-pressure measurement test technique has been used to do that, and then to analyze the dynamic responses of multi-degree-of-freedom system with non-linear or non-uniform mode shapes. Kareem (1982a, b) investigated the aerodynamic spectra in cross-wind of a square cross-section tall building with aspect ratio of 4 in both the urban and rural wind fields, and then gave the simplified calculation procedure considering aerodynamic damping ratio. Islam *et al*. (1990, 1992) researched the power spectra of along-wind, across-wind and torsional aerodynamic forces of a square cross-section building with aspect ratio of 8.33, and further offered a simplified calculation method for responses. Cheng and Kareem (1992) analyzed the influences of turbulence intensity and turbulence scale on the power spectrum of across-wind aerodynamic forces of a two-dimensional square pillar, and then derived empirical formulae of the along-wind aerodynamic admittance function and across-wind aerodynamic spectrum according to 27 kinds of flow field conditions.

Yeh and Wakahara (1997) studied the wind load power spectrum of the rectangular cross-section construction and then presented its mathematical expression. Lin *et al*. (2005) investigated in details the wind force spectra at different levels in the along-wind, cross-wind, and torsional directions of rectangular cross-section high-rise buildings with different aspect ratios. Unfortunately, they did not offer the mathematical formula. Liang *et al*. (2002, 2004) presented the mathematical models for across-wind and torsion force spectra of rectangular cylinders with various side ratios and aspect ratios at normal attack angle and then developed a calculation method to evaluate the wind-induced across-wind responses of rectangular tall buildings in frequency domain.

The above investigations on the characteristics and the mathematical models of the wind force spectra are mainly focused on some typical cross-section buildings. However, for that of buildings with complex shapes, few investigations have been made. In view of this, a 492 m super high-rise building with special shape is taken as an example to study the characteristics of wind force spectra in along-wind, cross-wind and torsion directions via a synchronous pressure measurement test. Then the mathematical models of them are proposed.

2. Wind tunnel experiment

2.1 Wind field simulation

The synchronous pressure measurement test of a 492 m high-rise building with a section varying along height and an inverted trapezoid at the top part (see Fig. 1) was carried out in the Atmospheric Boundary Layer Wind Tunnel, TJ-2, at Tongji University, China, with a working segment of 3 m in width, 2.5 m in height and 15 m in length, and with a range of wind speed from 1.0 m/s to 68 m/s. In this test, the reference wind speed was14m/s, which was monitored by Pitot tube at 1.2 m height in wind tunnel. In addition, an anemometer is used to measurethe turbulent wind velocities at different heights, including the reference point height.

The mean wind speed profile for terrain category C was simulated mainly by spires (see Fig. 1 (b)).The simulation result and the theoretical formula according to the Ministry of Construction P.R.China (GB50009 - 2006) are shown in Fig. 2(a). The turbulence intensity profile in along-wind was simulated by spires, grid and roughness elements (see Fig. 1 (b)). The simulation result and the theoretical formula according to the AIJ Recommendations for Architectural Institute of Japan (AIJ 1996) are shown in Fig.2 (b).The turbulence intensity profile in across-wind was only given the experimental results (see Fig. 2(c)). Fig. 3 shows the power spectra of fluctuating wind speeds in along-wind and across-wind directions at the reference point, as well as the Harris spectrum, the Davenport spectrum, the Karman spectrum and the fitted spectrum. It can be seen that the test results well agree with the Karman spectrum and the following fitted spectrum

$$nS_a / u_*^2 = a\, f_z^{\gamma} \Big/ \left(1 + b\, f_z^{1/m}\right)^{c\,m} \tag{1}$$

where a, b, m and γ are four fitting parameters (see Fig. 3);c is a constant coefficient, taken as5/3generally.

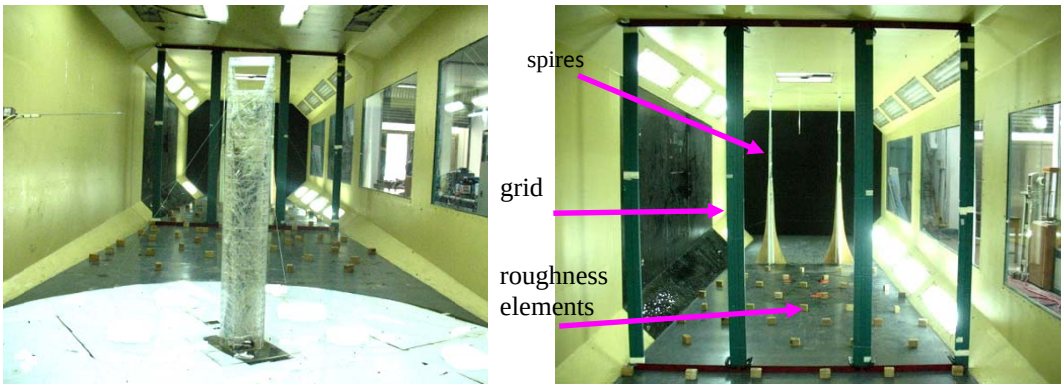

(a) rigid model in wind tunnel (b) wind field simulation

Fig. 1 Synchronous pressure measurement wind tunnel test of rigid model and wind field simulation

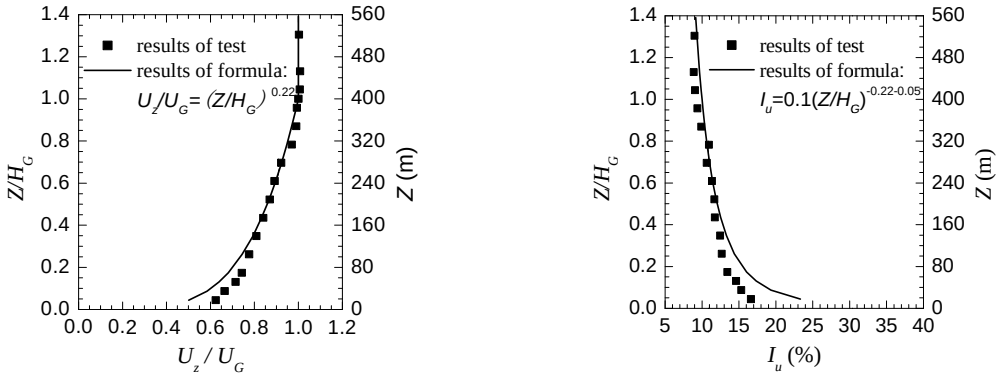

(a) Mean wind speed profile (b) Turbulence profile of along-wind

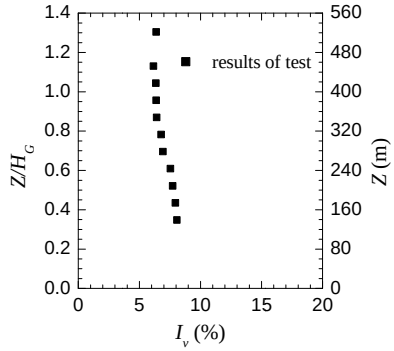

(c) Turbulence profile of across-wind

Fig. 2 The simulation results about the mean wind speed and turbulence profile of category C geomorphology

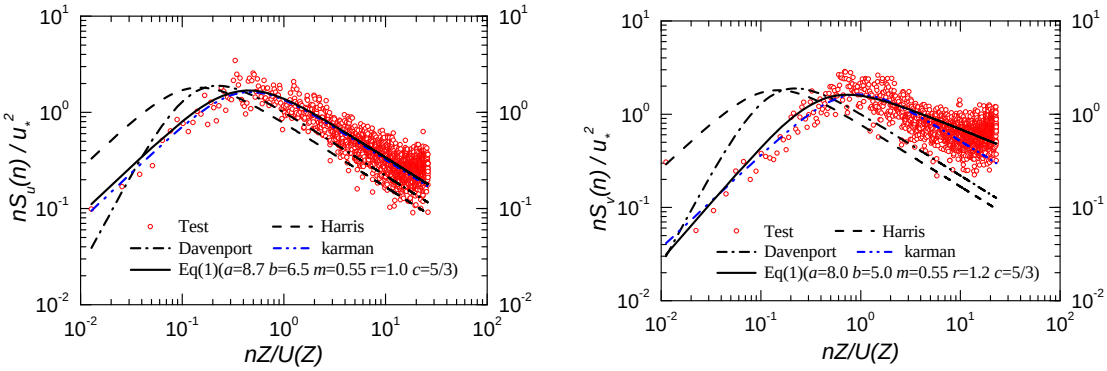

(a) Fluctuating wind spectrum of along-wind (b) Fluctuating wind spectrum of across-wind

Fig. 3 Fluctuating wind spectra of along-wind, across-wind on gradient high simulated in wind tunnel

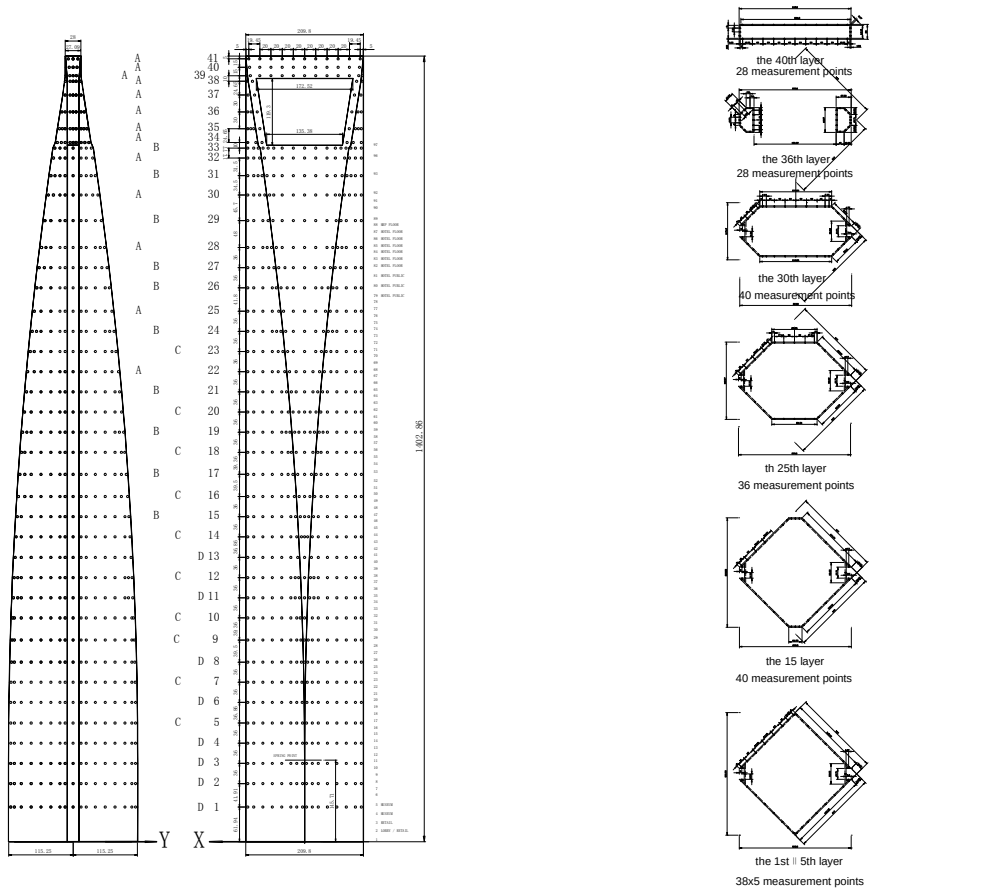

(a) side elevation (b) front elevation (c) cross-section on typical height

Fig. 4 The shape and measuring tap arrangement of façade and cross-sections of typical heights

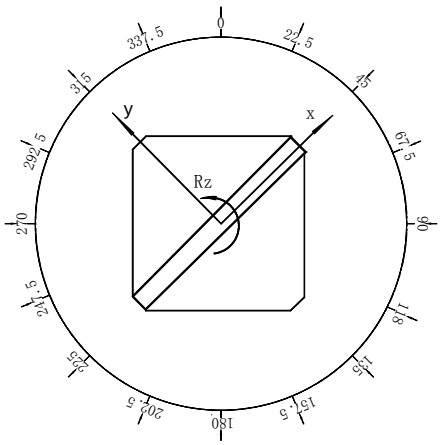

Fig. 5 Positions, wind direction and coordinate axis definitions of the model

2.2 Test model

The elevation profile, cross-sectional shapes of typical heights, and measurement tap arrangement of the 492 m high-rise building are shown in Fig. 4. Corresponding to the 1:350 length scales, the total height of this model is 1.4 m. In all, 1530 pressure measurement taps were distributed on 41 levels, which were numbered from bottom to top of the model. The 1~33 levels belong to the main body, and the 34~41 levels belong to the top part, in which the 34~38 levels are at the opening. Due to the limitations of the channels of the electronic scan valve, the signals of measuring taps could not be collected simultaneously at a time and should be divided into 4 groups of A, B, C and D, as shown in Fig. 4(a). Each pressure signal was sampled with 6000 data points at a frequency of 312.5 Hz.

2.3 Test conditions

The model orientation, wind direction and coordinate axis definition are shown in Fig. 5. The body axes include the X axis, the Y axis, and the RZ axis, which can be determined on the basis of the shape or the vibration modes of the structure. However, the wind axes include the along-wind direction and the across-wind direction, which are determined according to wind field direction. In this wind tunnel test, the wind pressure data are collected every 22.5^{o}, total 16 wind directions, as shown in Fig. 5.

3. Characteristics of wind force amplitudes at different levels of altitude

In aerodynamics, the dimensionless pressure coefficient time-history on the structural surface can be expressed as follows

$$C_{ij}(t)=\frac{p_{ij}(t)-p_{r\infty}(t)}{p_{r0}(t)-p_{r\infty}(t)} \tag{2}$$

Where $C_{ij}(t)$ is the dimensionless pressure coefficient time-history at the j^{th} measuring tap in the i^{th} levels of altitude, which takes the dynamic pressure at the reference point as reference pressure; $p_{ij}(t)$ is the wind pressure time-history at the j^{th} measuring tap in the i^{th} levels of altitude; $p_{r0}(t)$ and $p_{r\infty}(t)$ are the synchronous measurement total pressure and static pressure time-histories at the reference point, respectively ; $p_{r0}(t)-p_{r\infty}(t)$ express the dynamic pressure time-history of reference point.

In order to eliminate the distortions of tubing system, the experimental method (Irwin *et al*. 1979) and analytical method (Holmes and Lewis 1987) were proposed. In this paper, the wind pressures of measuring tap are revised by the analytical method.

Subsequently, the wind force coefficient time-history of each measurement level (also call measuring layer, same as the following) can be calculated by the following integral summation formulae

$$C_{x_i}(t)=\sum_{j=1}^{m_i}C_{ij}(t)\cdot A_{ij}\cdot\cos(\alpha_{ij})\cdot\sin(\beta_{ij})/(B_{x_i}h_i) \tag{3a}$$

$$C_{y_i}(t)=\sum_{j=1}^{m_i}C_{ij}(t)\cdot A_{ij}\cdot\sin(\alpha_{ij})\cdot\sin(\beta_{ij})/(B_{y_i}h_i) \tag{3b}$$

$$C_{Rz_i}(t)=\sum_{j=1}^{m_i}\left[C_{ij}(t)\cdot A_{ij}\cdot\sin(\alpha_{ij})\cdot\sin(\beta_{ij})\cdot x_{ij}-C_{ij}(t)\cdot A_{ij}\cdot\cos(\alpha_{ij})\cdot\sin(\beta_{ij})\cdot y_{ij}\right]/(B_{x_i}B_{y_i}h_i) \tag{3c}$$

where, $C_{x_i}(t)$, $C_{y_i}(t)$, $C_{Rz_i}(t)$ are the dimensionless wind force coefficient time-histories of the i^{th} measuring level along X, Y axes, and around Z axis respectively; A_{ij} is the control area of the j^{th} measuring tap in the i^{th} level of altitude; α_{ij} is the angle (clockwise) between the projection in XOY plane of the normal at the j^{th} measuring tap in the i^{th} levels of altitude and the X axis; β_{ij} is the angle between the normal at the j^{th} measuring tap in the i^{th} levels of altitude and Z axis; h_i is effective height of the i^{th} measuring level; B_{x_i} and B_{y_i} are the characteristic width of the i^{th} measuring level perpendicular to the X and Y axes respectively; x_{ij} and y_{ij} are X and Y coordinates of the j^{th} measuring tap in the i^{th} level of altitude respectively; m_i is the number of measuring taps in the i^{th} level of altitude.

The mean value of wind force coefficients of the i^{th} levels of altitude along X, Y axes and around Z axis are recorded as $C_{x_i}^{mean}$, $C_{y_i}^{mean}$ and $C_{Rz_i}^{mean}$, respectively. The root-mean-square (RMS)of fluctuating wind force coefficients along X, Y axes and around Z axis are recorded as $C_{x_i}^{rms}$, $C_{y_i}^{rms}$ and $C_{Rz_i}^{rms}$

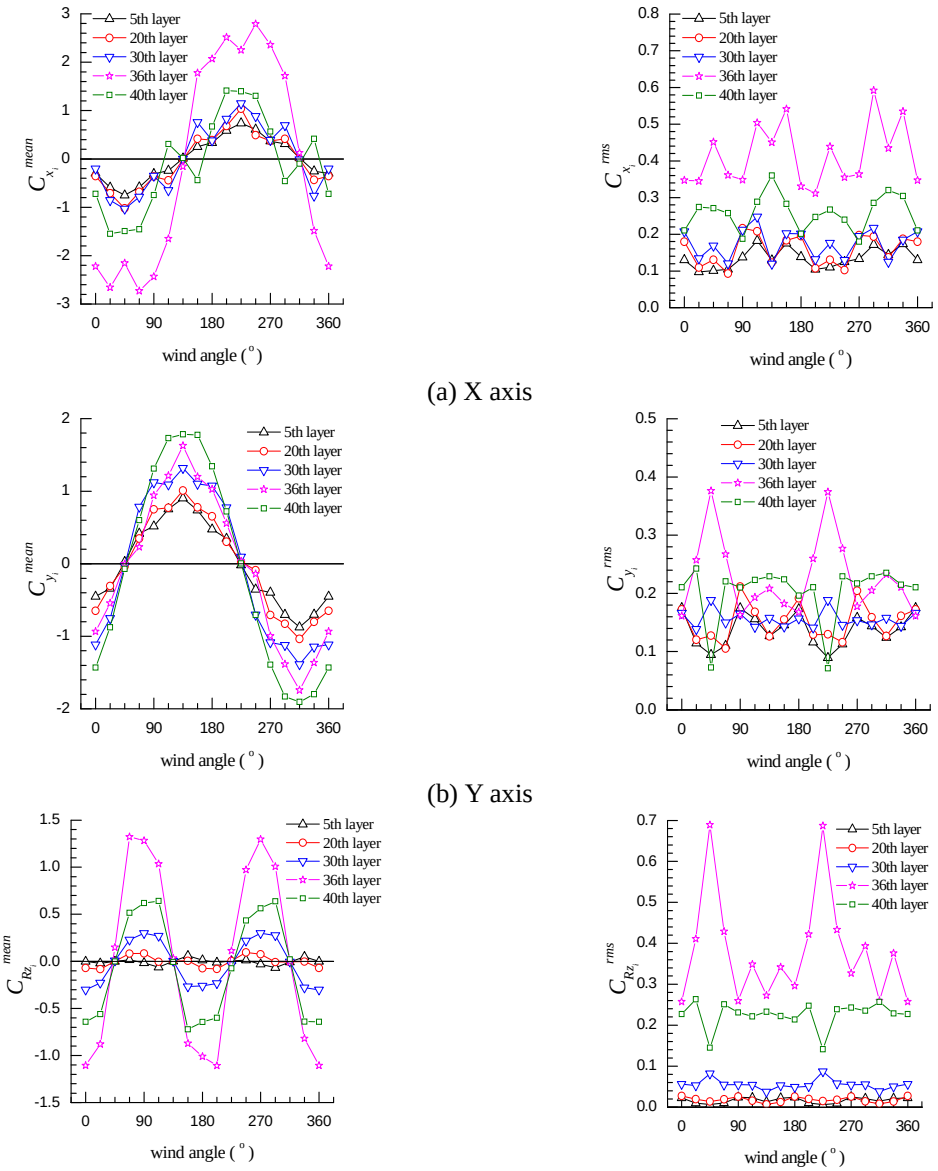

Fig. 6 The wind force coefficients varying with the wind angle and the height

Fig. 6 shows the mean and RMS wind force coefficients of X axis, Y axis and RZ axis of typical levels of altitude varying with wind angle (0º~360º). The results of 5th, 20th, 30th, 36th, 40th levels represent that of the lower, middle and upper part of the main body (i.e., 1-32 levels), the opening and the top of the structure, respectively.

The results in Fig. 6 show us the following features: the absolute values of mean and RMS wind force coefficients increase along with the increase of the height except for a few wind direction angles; the absolute values of mean and RMS wind force coefficients of X and RZ axis at the opening of the top part are greatly larger than that of the other levels; the maximum absolute mean wind force coefficients of X axis of the main body appears in about 45º wind direction(equivalent to across-wind direction), that of Y axis appears in 315º wind direction (equivalent to across-wind direction), and that of RZ axis appears in 0ºwind direction.

As the structure is symmetrical, only three wind angles such as 315º, 0°, and 45° are taken as examples to analyze the numeric value and variation characteristics of wind force coefficients along the height of the structure.

Fig. 7(a) shows the mean and RMS wind force coefficients of X axis (body axis) varying along height of the model in wind direction of 315º, 0º and 45º.The mean wind force coefficients in Fig. 7(a) show us the following features: in wind direction of 315º (equivalent to across-wind direction), the mean wind force coefficients of the main structure vary little along height and are close to zero, but that of the opening in the top part increase slightly; in wind direction of 0º, the mean wind force coefficients of the main structure vary little along height, but that of the opening in the top part increase rapidly; in wind direction of 45º(equivalent to along-wind direction), the absolute values of mean wind force coefficients of the main structure increase along with the increase of the height, and that of the opening in the top part increase rapidly, and that of the top of structure also increase for the influence of the three-dimensional flow. The RMS wind force coefficients in Fig. 7(a) show us the following features: in wind direction of 315º (equivalent to across-wind direction),the RMS wind force coefficients of the main structure vary little along height, but that of the opening in the top part increase greatly for structural cross-section turning smaller with large opening area; in wind direction of 0º, the RMS wind force coefficients at the main structure increase along the height, but at those measuring levels close to the platform and the top, they decrease slightly for the three-dimensional flow. At the opening in the top part, they increase greatly; in wind direction of 45º (equivalent to along-wind direction), the RMS wind force coefficients of main structure increase along the height, but those at opening of the top part increase greatly.

Fig. 7(b) shows the mean and RMS wind force coefficients of Y axis (body axis) varying along height of the model in wind direction of 315º, 0º and 45º. The mean wind force coefficients in Fig. 7(b) show us the following features: in wind direction of 315º(equivalent to along-wind direction), the absolute values of mean wind force coefficients of main structure increase along with the increase of height, which is similar to the mean wind pressure profile, and those approach to the edge of opening and the edge of structural top decrease for the influence of the three-dimensional flow; in wind direction of 0º,the change regulation of the mean wind force coefficients along height is similar to wind direction 315º in addition to a smaller value; in wind direction of 45º (equivalent to across-wind direction), the mean wind force coefficients of structure vary little along height and are close to zero. The RMS wind force coefficients in Fig. 7(b) show us the following features: in wind direction of 315º (equivalent to along-wind direction) and 0º, the RMS wind force coefficients of structure increase slightly along height; in wind direction of 45º (equivalent to across-wind direction), the RMS wind force coefficients increase along with the increase of the height, and those at the opening of the top part increase rapidly, however, those at the edge of structural top decrease a lot.

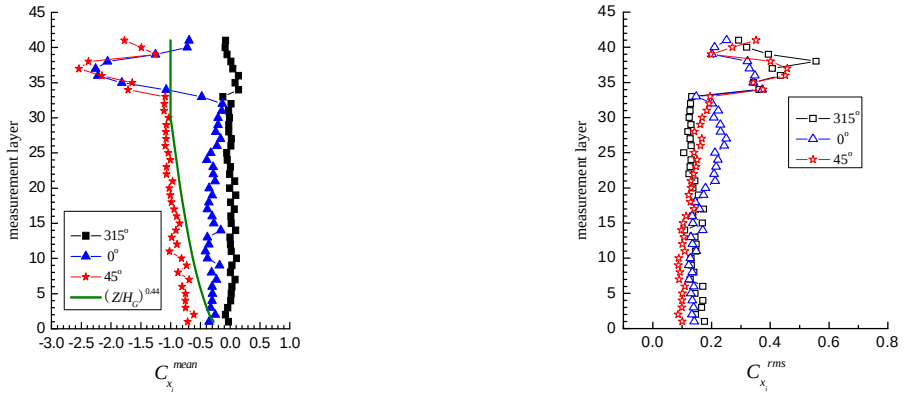

(a) X axis

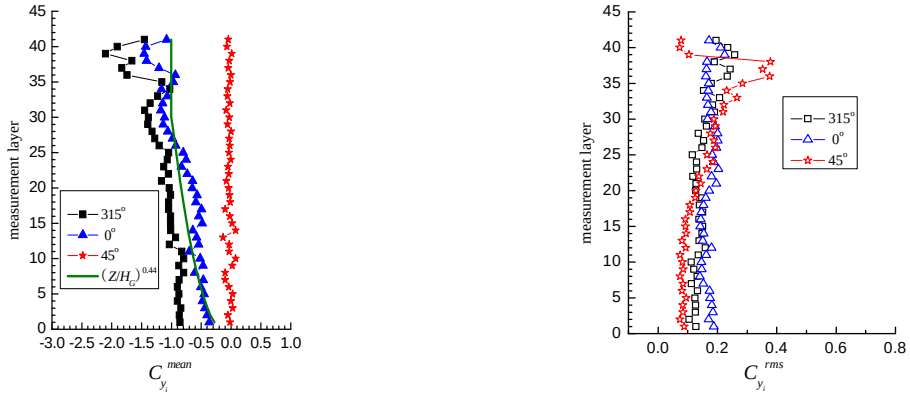

(b) Y axis

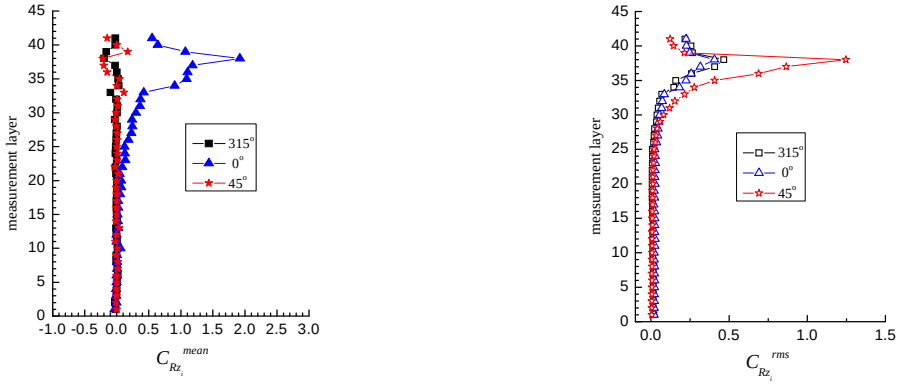

(c) RZ axis

Fig. 7 The mean and RMS wind force coefficients of body axis varying along height of the model

Fig. 7(c) shows the mean and RMS wind force coefficients of RZ axis (body axis) varying along height of the model in wind direction of 315º, 0º and 45º. The mean wind force coefficients in Fig. 7(c) show us the following features: in wind direction of 315º and 45º, the mean wind force coefficients of structure vary little along height and are close to zero for the symmetry of structural shape; in wind direction of 0º, the absolute values of mean wind force coefficients of structure increase along with the increase of height and increase quickly upper 25th level and increase significantly at the opening of structural top part and its edge. The RMS wind force coefficients in Fig. 7(c) show us the following features: in wind direction of 315º, 45º and 0º, the RMS wind force coefficients of structure vary little along height under 25th measuring level, however, they increase quickly above 25th measuring level and increase greatly at the opening of structural top part and its edge. These characteristics are particularly obvious in the 45º wind direction.

4. Characteristics of wind force spectra at different levels of altitude

The standardized power spectra of wind force coefficients at some crucial measurement levels of altitude on this extra-high building in wind direction of 315º, 0º, and 45º are analyzed in detail in this section.

(1) 315º wind direction

Figs. 8(a)-8(f) show the standardized spectra of wind force coefficients at some crucial measurement levels of X axis, Y axis, and RZ axis in wind direction of 315º. For this wind direction, X and Y axis are equivalent to across-wind and along-wind, respectively.

Figs. 8(a) and 8(b) show the standardized wind force coefficient spectra at different levels of X axis (cross-wind). In the main body (see Fig. 8(a)), the standardized wind force coefficient spectra have the tendency that the power spectra become flat, the basic frequency increases, and the energy in high-frequency increases with height increasing. meanwhile, the reduced frequency at peak value of $f_c = fB/U_G$ is about 0.137, where the vortex shedding energy is stronger. At the top part (see Fig. 8(b)), the standardized wind force coefficient spectra are comparatively flat, their basic frequencies are nearly 0.27 and 1.20, and the energy in high-frequency is much higher. However, at the edges of aperture (measuring levels of 34 and 38), the basic frequency is close to 1.20, the energy in low-frequency becomes lower, and the energy in high-frequency becomes higher.

Figs. 8(c) and 8(d) show the standardized wind force coefficient spectra at different levels of altitude of Y axis (along-wind). It can be seen from the figures that the standardized wind force coefficient spectra are more flat and similar to the wind spectrum, and the energy in high-frequency range increases along height, otherwise, in the main body, the basic frequency is close to 0.137,at the top part, the energy increases near the reduced frequency of 1.20.

Figs. 8(e) and 8(f) show the standardized wind force coefficient spectra at different levels of altitude of RZ axis (torsion). In the main body (see Fig. 8(e)), with the height increasing, the standardized wind force coefficient spectra tend to be flat and the energy in high-frequency increases, moreover, the reduced frequency at peak value of $f_c = fB/U_G$ is about 0.137. At the top part (see Fig. 8(f)), the standardized wind force coefficient spectra are comparatively flat, their basic frequencies are nearby 0.137 and 1.20, and the energy in high-frequency is much higher. Generally, the varying properties of standardized wind force coefficient spectra round Z axis (torsion) at different levels are similar to those of X axis along height.

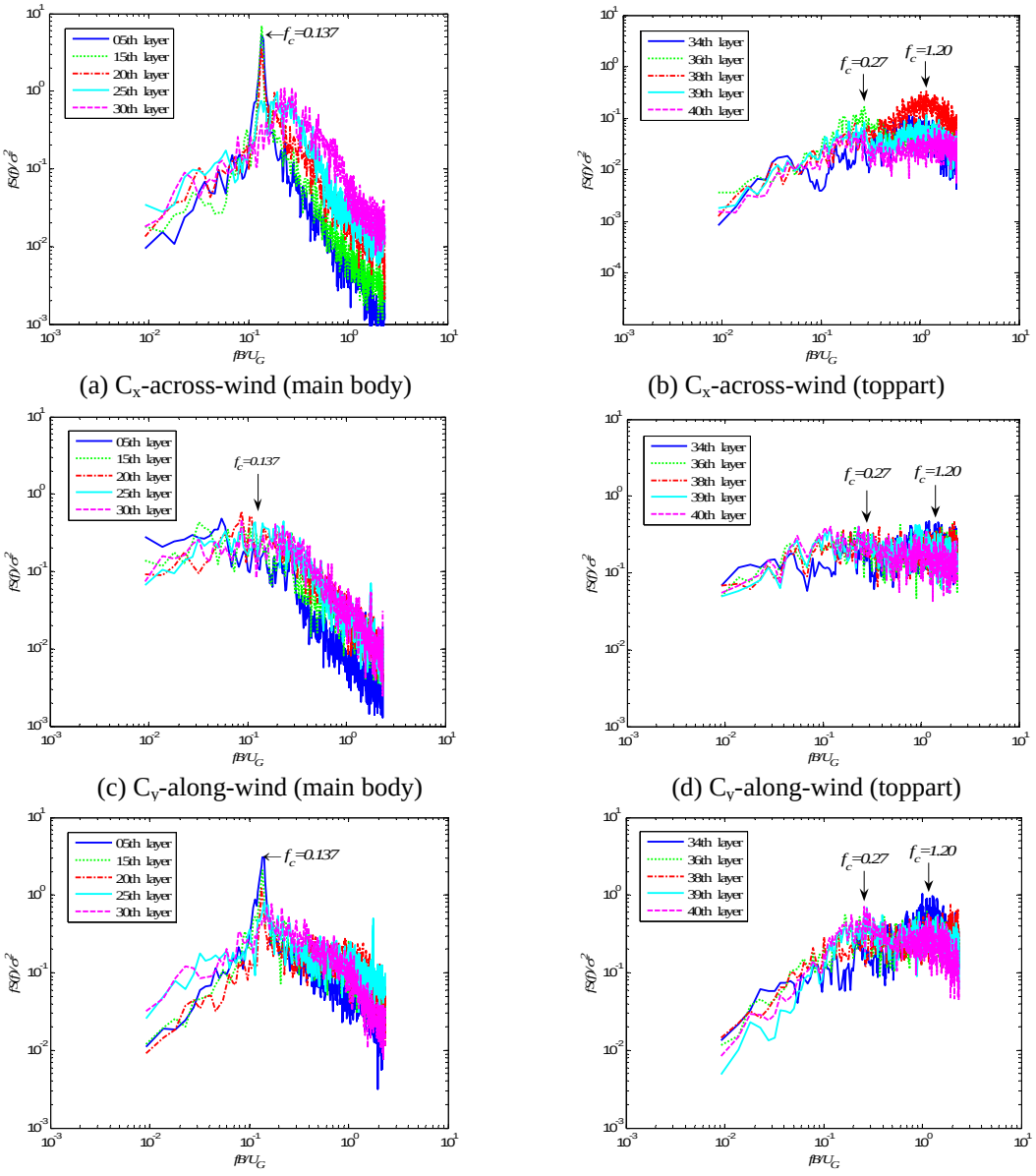

(a) C_x-across-wind (main body)

(b) C_x-across-wind (toppart)

(c) C_y-along-wind (main body)

(d) C_y-along-wind (toppart)

(e) C_{Rz}-torsion (main body)

(f) C_{Rz}-torsion (toppart)

Fig. 8 Normalized power spectra of wind force coefficients in wind direction of 315°

(2) 0° wind direction

Figs. 9(a) - 9(f) show the standardized spectra of wind force coefficients at some crucial measurement levels of X axis, Y axis, and RZ axis in wind direction of 0°. At this time, X and Y axis is neither along-wind nor across-wind.

Figs. 9(a) and 9(b) show the standardized wind force coefficient spectra at different levels of X

axis. Relative to that of the main body (see Fig. 9(a)), the spectra at the top part (see Fig. 9(b)) are flat, more uniform of spectral distribution, and much higher energy in high-frequency. The reduced frequencies as $f_c = fB/U_G$ at peak value of spectra of the main body are about 0.21, where the vortex shedding energy is stronger., There is also a stronger energy at reduced frequency 1.05 of the top part except for high energy in basic frequency of spectra near 0.21.

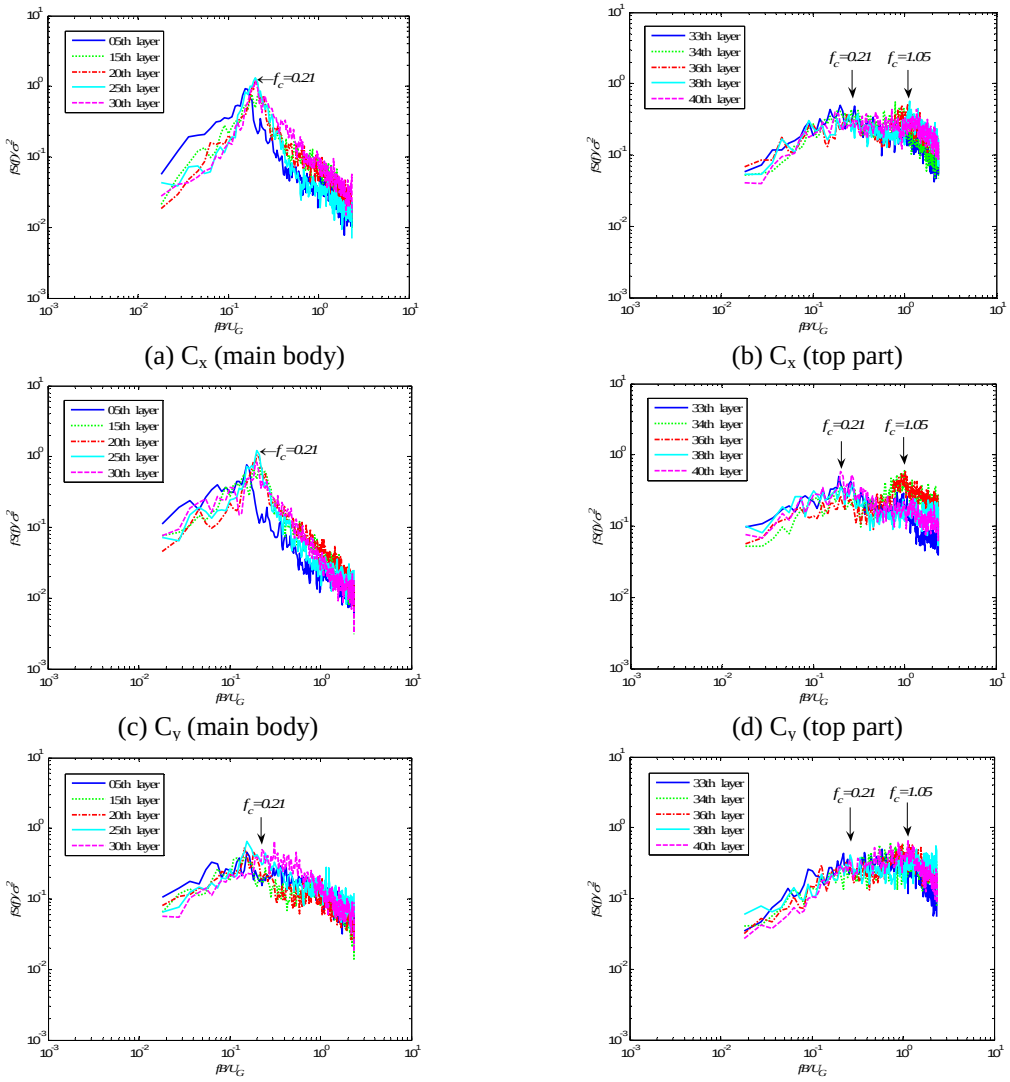

(a) C_x (main body)

(b) C_x (top part)

(c) C_y (main body)

(d) C_y (top part)

(e) C_{Rz}-torsion (main body)

(f) C_{Rz}-torsion (top part)

Fig. 9 Normalized power spectra of wind force coefficients in wind direction of 0°

(note： f_c is reduced frequency, B is the characteristics width perpendicular to the Y axis, U_G is the gradient wind speed)

Figs. 9(c) and 9(d) show the standardized wind force coefficient spectra at different levels of altitude of Y axis. It can be seen from the figures that the standardized wind force coefficient spectra of Y axis are similar to that of X axis.

Figs. 9(e) and 9(f) show the standardized wind force coefficient spectra at different levels of altitude of RZ axis (torsion). It can be seen from the figures that the proportion of low frequency energy of main body is larger than that of the top part, however, the proportion of high frequency energy at the top part increase and the high basic reduced frequency is near 1.05.

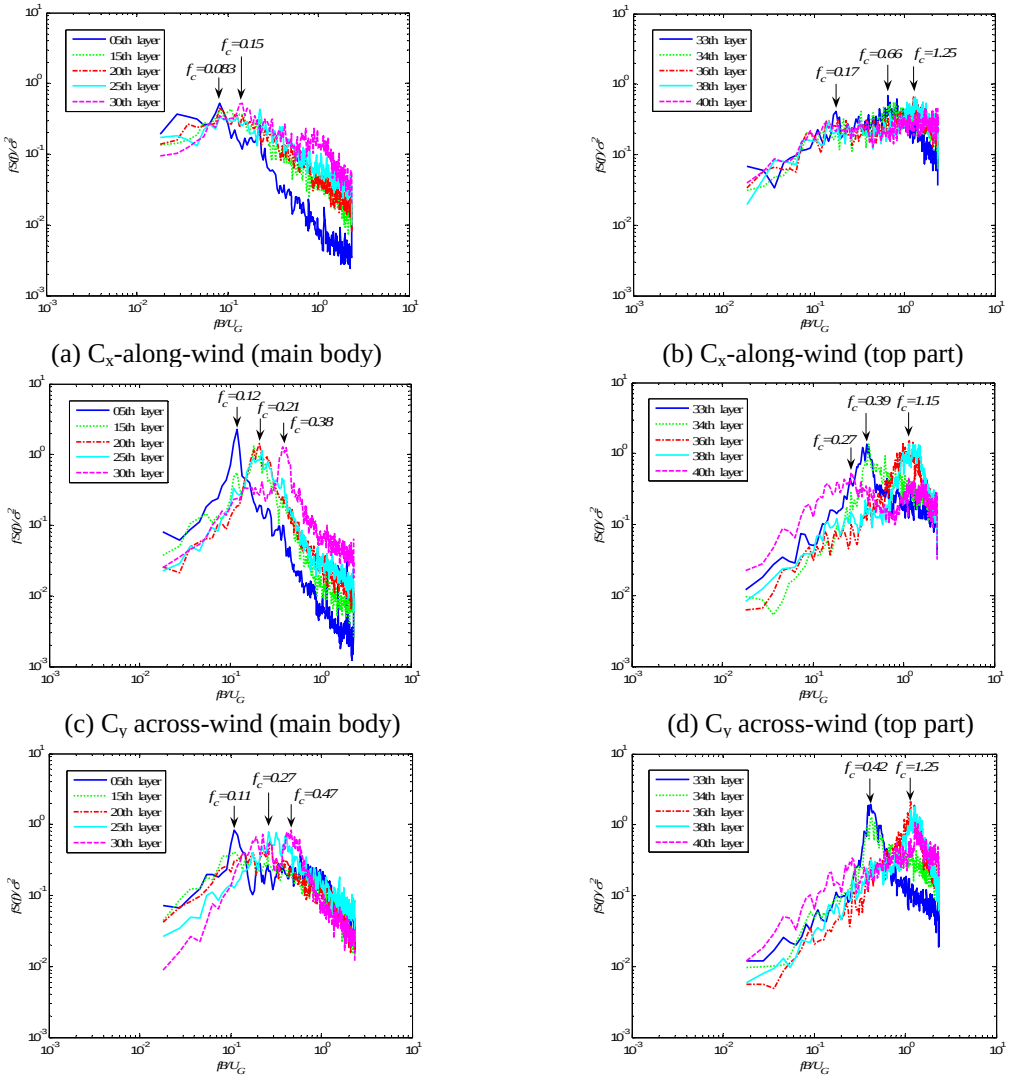

(a) C_x-along-wind (main body)

(b) C_x-along-wind (top part)

(c) C_y across-wind (main body)

(d) C_y across-wind (top part)

(e) C_{Rz}-torsion (main body)

(f) C_{Rz}-torsion (top part)

Fig. 10 Normalized power spectra of wind force coefficients in wind direction of 45°

(note： f_c is reduced frequency, B is the characteristics width perpendicular to the Y axis, U_G is the gradient wind speed)

(3) 45º wind direction

Figs. 10(a) - 10(f) show the standardized spectra of wind force coefficients at some crucial measurement levels of X axis, Y axis, and RZ axis in wind direction of 45º. For this wind direction, X and Y axis are equivalent to along-wind and across-wind, respectively.

Figs. 10(a) and 10(b) show the standardized wind force coefficient spectra at different levels of X axis (along-wind). It can be seen from the figures that, the proportions of high frequency energy of the main body increase along with the increase of height, and that of the top part are larger than that of the main body.

Figs. 10(c) and 10(d) show the standardized wind force coefficient spectra at different levels of altitude of Y axis (across-wind). It can be seen from the figures that the reduced frequencies at peak value of spectra as well as the proportions of high frequency energy increase along with the increase of height, and the proportions of high frequency energy at the top part are much larger than that in the main body.

Figs. 10(e) and 10(f) show the standardized wind force coefficient spectra at different levels of altitude of RZ axis (torsion). It can be seen from the figures that the reduced frequencies at peak value of spectra increase along with the increase of height, and the proportions of high frequency energy of the top part are larger than that of the main body.

5. Mathematical expressions of wind force spectra

Wind force spectra at different levels of altitude are indispensable part of constructing wind load power spectrum matrix and calculating wind-induced responses, moreover, the mathematical expressions can more clearly display the composition of power spectra, therefore, the mathematical expressions of wind force spectra would be discussed in details according to the their characteristics shown in section 4.

As shown in section 4, the standardized power spectra of wind force coefficients along height in wind direction of 315º are regular for the symmetry of shape and the consistency of body axis and wind axis, thus the mathematical expressions of them in wind direction of 315º are taken as example to discuss in this section.

5.1 X axis (across-wind)

The mathematical expression of across-wind force spectrum in AIJ (1996) , which adopts the research results of Marukawa *et al*. (1992), is as follows

$$\frac{fS(f)}{\sigma^2} = \sum_{j=1}^{N} \frac{4K_j(1+0.6\beta_j)\beta_j}{\pi} \cdot \frac{(f/f_{cj})^2}{\left[1-(f/f_{cj})^2\right]^2 + 4\beta_j^2(f/f_{cj})^2} \quad , N=1 \ , \ 2 \tag{4}$$

where K_j expresses the contribution of the j^{th} force spectrum coefficients; β_j is a constant of the j^{th} associated with bandwidth; f_{cj} is the j^{th} frequency at peak.

Referring to Eq. (4), a mathematical formula of across-wind force spectrum was provided by Gu and Quan (2004)

$$\frac{fS(f)}{\sigma^2}=\sum_{j=1}^{N}\frac{S_{cj}\beta_j(f_c/f_{cj}^*)^{\alpha_j}}{\left[1-(f_c/f_{cj}^*)^2\right]^2+\beta_j(f_c/f_{cj}^*)^2}\ ,\ N=1\ ,\ 2 \tag{5}$$

where f_{cj}^*, β_j, S_j and α_j are parameters to be determined, which identify the peak value abscissa, peak value ordinate, bandwidth and skewness of a power spectrum curve, respectively.

By comparison, Eqs. (4) and (5) are similar, but the latter is more intuitively to express the abscissa of peaks, the ordinate of peaks, bandwidth and skewness of the power spectrum. Therefore, in this paper, Eq. (5) is accepted to fit the wind force spectrum curves at typical measuring levels, as shown in Fig. 11.It can be seen in figure that when the peak value of the vortex shedding of power spectrum is very large but with narrow band, the fitting effects are good at peak value but bad at other frequency bands, being smaller. When the power spectrum includes two basic frequencies, superposition of two formulae can gain better fitting effect, for instance the measurement levels of 34-41.

By observing Fig. 8(a) one can find that the force spectrum curves of X axis (across-wind) on the main structural part are composed with two parts-one part is caused by turbulent flow, and the other is caused by vortex shedding. In other words, the former is closer to wind spectrum like Eq. (1), and the later is closer to a peak function.

Therefore, the mathematical formula of wind force spectrum in X axis (across-wind) direction can be superimposed by some wind spectra functions and a peak function, as following

$$\frac{fS(f)}{\sigma^2}=\sum_{j=1}^{N}\frac{a_j f_c}{\left(1+b_j f_c^{c_j}\right)^{d_j}}+A_1\exp\left[-(f_c-B_1)^2/C_1^2\right]\ ,\ N=1\ ,\ 2 \tag{6}$$

where $f_c=\dfrac{fB}{U_G}$; a_j, b_j, c_j, d_j, A_1, B_1, $C_1$are fitting parameters to be determined（j=1，2）.

Eq. (6) is used to fit the wind force power spectrum curves at measuring levels of 5, 10, 15, 20, 23, 25, 30, 36 and 40, respectively, as partially shown in Fig. 11, and the fitting parameters are listed in Table1.Fig. 9 shows that the proposed mathematical formulae of wind force spectra in X axis (across-wind) direction, Eq. (6), are well matching the test results. By observing the characteristics and the fitting parameters of the wind force spectrum curves one can found that the fitting parameters has certain rule for structural cross-section changing along height, thus, they can be summarized by several formulae.

When the fitting parameters of each wind force spectrum in Table 1 are put into same coordinate, respectively, as shown in Fig. 12, the following formulae can be used to fit them

$$a_1=\frac{1}{0.459(H_z/H_G-0.803)^2+0.471}+0.961(H_z/H_G) \tag{7a}$$

$$b_1=\left[408(H_z/H_G)^{0.012(H_z/H_G)^{-5.24}}+67.3\right]^{10} \tag{7b}$$

$$c_1=\frac{1}{0.047-0.029(H_z/H_G)-0.0163(H_z/H_G)^2+0.0194(H_z/H_G)^3} \tag{7c}$$

$$d_1 = 0.072 - 0.22(H_z/H_G) - 0.0656(H_z/H_G)^2 + 0.097e^{(H_z/H_G)} \tag{7d}$$

$$A_1 = \frac{5.65 - 3.19(H_z/H_G)}{1 + 1.82\times10^7 (H_z/H_G)^{64}} \tag{7e}$$

$$B_1 = 0.137 \tag{7f}$$

$$C_1 = \frac{0.0029}{1 + e^{58.5(H_z/H_G - 0.392)}} + 0.00618 \tag{7g}$$

For the complexity of the wind force spectra at top part, they are better to be fitted separately. However, they also can be fitted altogether (except the opening edge) in order to facilitate calculation, as shown in the last figure of Fig. 11.

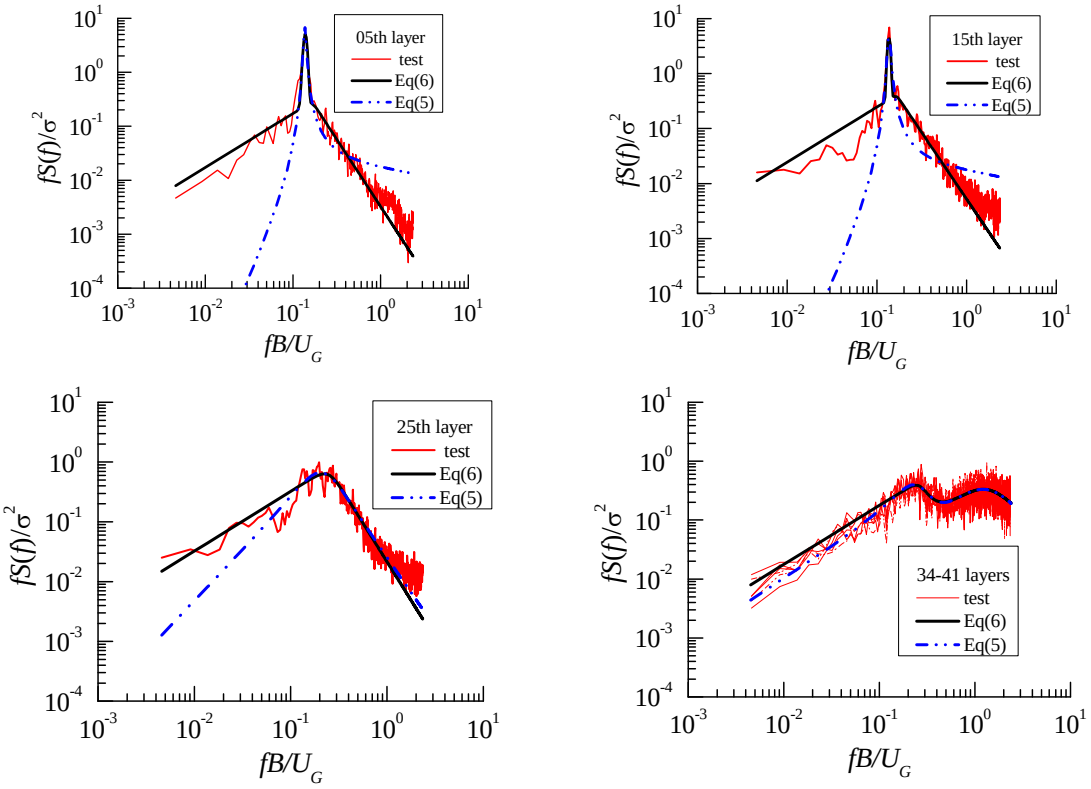

Fig. 11 Fitting results about the wind force spectra of X-axis at typical measurement levels in wind direction of 315°

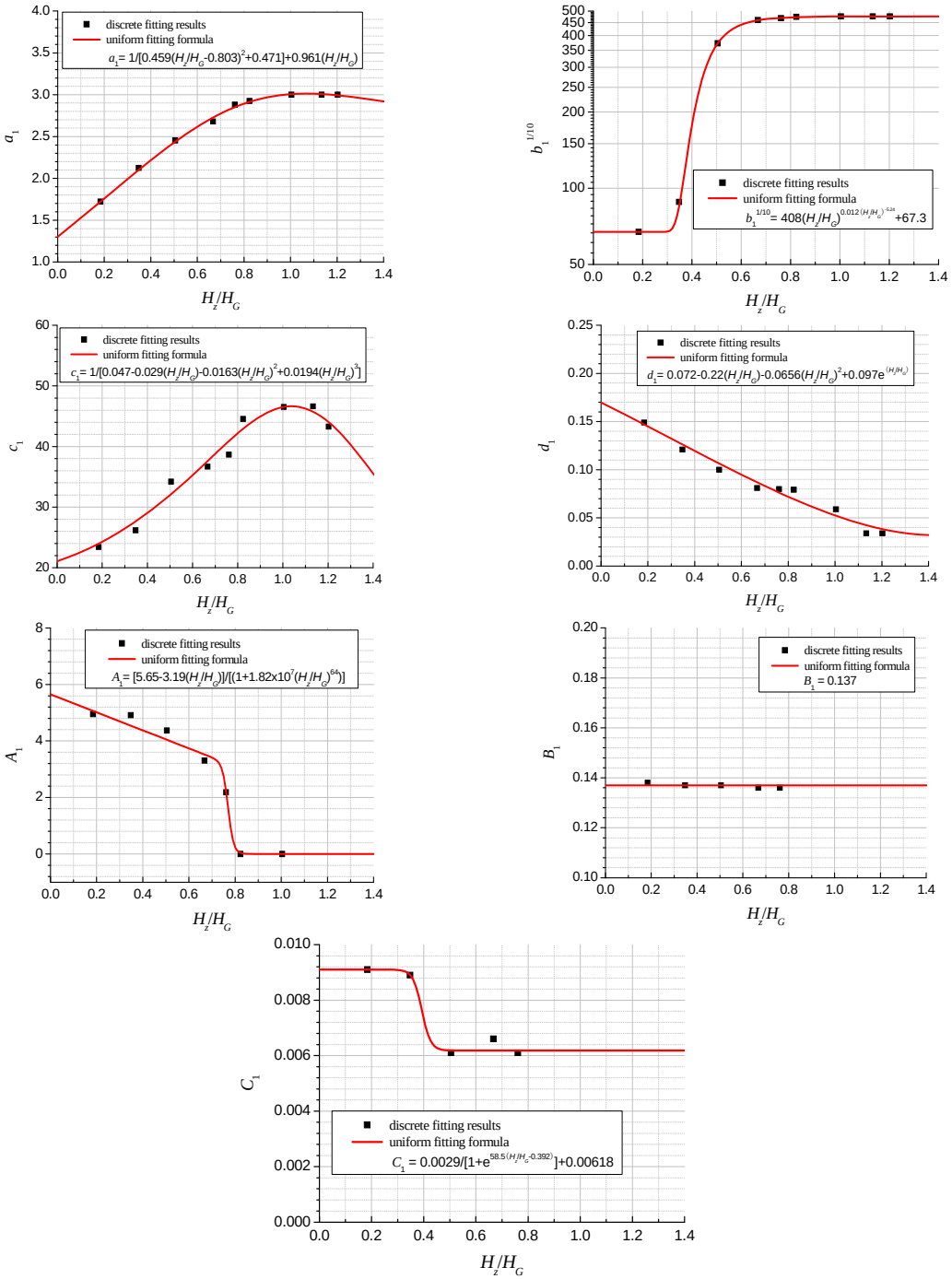

Fig. 12 Fitting results about the fitted parameters of wind force spectra of X-axis in wind direction of 315º

5.2 Y axis (along-wind)

Figs. 8(c) and 8(d) show that the wind force spectra of Y axis (along-wind) have no obvious vortex shedding peak, therefore, they can be expressed by the following formula

$$\frac{fS(f)}{\sigma^2}=\sum_{j=1}^{N}\frac{a_j f_c}{\left(1+b_j f_c^{c_j}\right)^{d_j}}\ ,\ N=1\ ,\ 2 \tag{8}$$

Where $f_c=\dfrac{fB}{U_G}$; a_j, b_j, c_j, d_j are fitting parameters to be determined (j=1 , 2).

By observing on power spectra of each measuring level obtained through experiment one can see that the power spectra at measurement levels of 1-12, 13-24, 25-32, and 34-41(except for the opening edge) are similar respectively, therefore, they can be divided into above 4 groups to carry out fitting, as shown in Fig.13,and the related fitting parameters are listed in Table 2. Additionally, Fig. 13 and Table 2 also give the fitting results with Eq. (5). Fig. 13 shows that for such wide-band power spectra of the Y-axis (across-wind), both Eqs. (5) and (8) well match the test results.

Table 1 Fitting results about wind force spectra of X-axis at typical measurement levels in wind direction of 315°

direction	measurement level	H_z (m)	a_1	b_1	c_1	d_1	A_1	B_1	C_1	
	5	0.212	1.721	1.9E18	23.41	0.149	4.950	0.138	0.0091	
	10	0.400	2.125	2.3E19	26.17	0.121	4.913	0.137	0.0089	
	15	0.580	2.4542	5.2E25	34.20	0.100	4.370	0.137	0.0061	
X axis	20	0.767	2.680	4.3E26	36.67	0.081	3.305	0.136	0.0066	
	23	0.875	2.88	5.1E26	38.67	0.080	2.1851	0.136	0.0061	
	25	0.947	2.925	5.8E26	44.53	0.079	0	/	/	
	30	1.155	3.000	6.0E26	46.53	0.059	0	/	/	
			a_1	b_1	c_1	d_1	a_2	b_2	c_2	d_2
	34-41	/	0.3523	0.2545	4.897	0.496	1.418	3.07E7	12.876	0.382

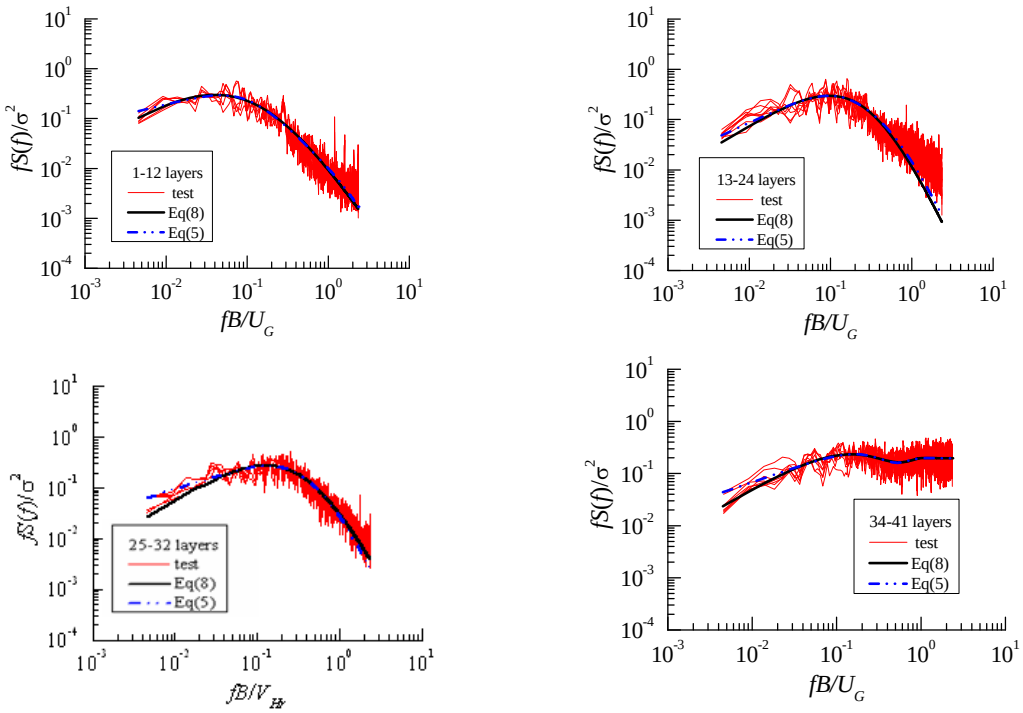

Fig. 13 Fitting results about the wind force spectra of Y-axis at each group of measurement levels in wind direction of 315°

Table 2 Fitting results about wind force spectra of Y-axis at each group of measurement levels in wind direction of 315°

direction	measurement level		a_1	b_1	c_1	d_1		f_{c1}^*	β_1	S_1	α_1
Y axis	1-12	Eq. (8)	28.7	6.75	0.871	3.93	Eq. (5)	0.51	0.030	30.96	0.405
	13-24		7.92	4.81	1.203	3.72		0.300	0.145	7.606	0.746
	25-32		6.10	3.20	1.107	3.69		0.498	0.107	6.415	0.746
	34-41	Eq. (8)	a_1	b_1	c_1	d_1	a_2	b_2	c_2	d_2	
			0.21	2.09	11.65	0.087	5.39	0.0056	0.840	1225	
		Eq. (5)	f_{c1}^*	β_1	S_1	α_1	f_{c2}^*	β_2	S_2	α_2	
			0.72	9.18	0.080	0.559	0.685	1.636	0.090	4.19	

5.3 RZ axis (torsion)

It can be seen from Fig.8 that the wind force spectra at different levels of altitude around Z axis (rotation) are similar to those of X axis (cross-wind). Therefore, they can also be expressed as the superimposed formula

$$\frac{fS(f)}{\sigma^2}=\sum_{j=1}^{N}\frac{a_j f_c}{\left(1+b_j f_c^{c_j}\right)^{d_j}}+A_1\exp\left[-(f_c-B_1)^2/C_1^2\right]\ ,\ N=1\ ,\ 2 \tag{9}$$

where $f_c=\dfrac{fB}{U_G}$; a_j, b_j, c_j, d_j, A_1, B_1, $C_1$are fitting parameters to be determined (j=1 , 2)

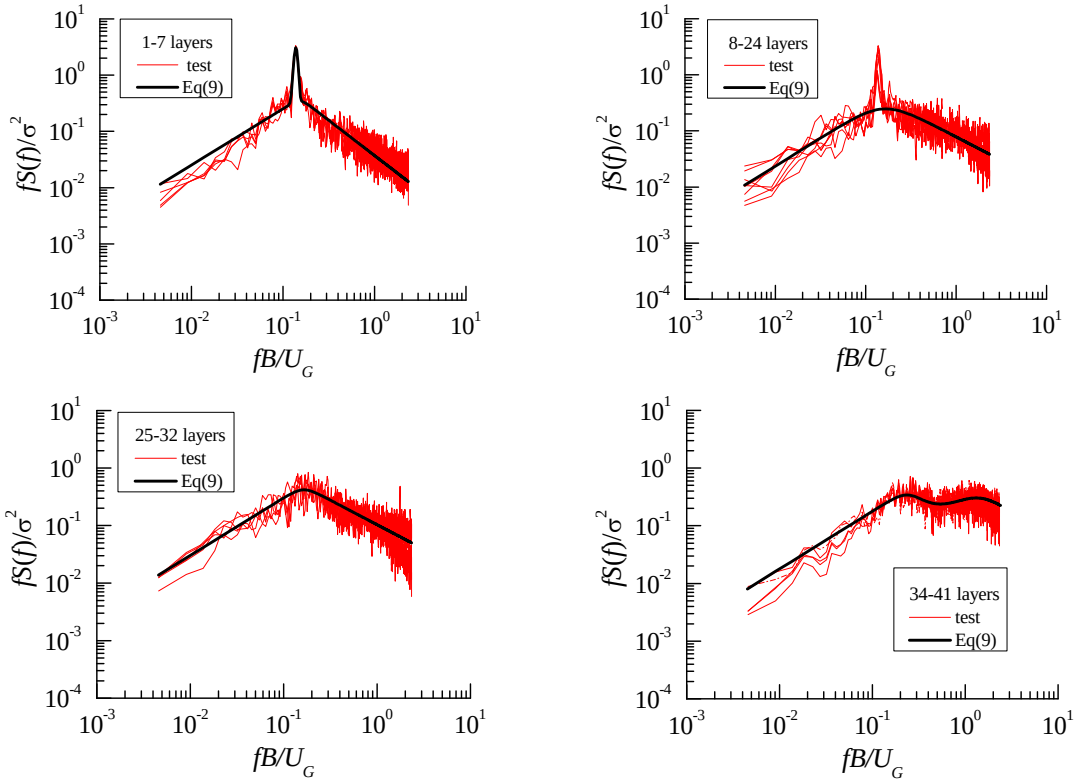

Fig. 14 Fitting results about the wind force spectra of RZ-axis at each group of measurement levels in wind direction of 315°

By observing on the power spectra at each measuring level obtained through experiment one can see that power spectra at measurement levels of 1-7, 8-24 (ignoring the peak part), 25-32, and 34-41(except for the edge of opening) are similar respectively, therefore, they can be divided into above4 groups to carry out fitting, as shown in Fig. 14, and the fitting parameters are listed in Table 3. For the peak of power spectra at measuring levels of 8-24, Table 3 lists the fitting results at measuring levels of 10, 14, 18, 20, and 23. When the fitting parameters of A_1, B_1, and C_1 are put into same coordinates respectively, as shown in Fig. 15, the following formulae can be used to fit them

$$A_1 = e^{[1.15+1.06(H_z/H_G)^{2.5}-6.03(H_z/H_G)^3]} \tag{10a}$$

$$B_1 = 0.137 \tag{10b}$$

$$C_1 = 0.00884 - \frac{0.00294}{1+e^{-(H_z/H_G-0.605)/0.00497}} \tag{10c}$$

For the complexity of the wind force spectra at top part, they are better to be fitted separately. However, they also can be fitted altogether (except the opening edge) in order to facilitate calculation, as shown in the last figure of Fig. 14.

Table 3 Fitting results about wind force spectra of RZ-axis at each group of measurement levels in wind direction of 315°

direction	measurement level		H_z(m)	a_1	b_1	c_1	d_1	A_1	B_1	C_1	
RZ axis	1-7		/	2.522	3E10	12.89	0.175	2.809	0.138	0.0088	
	8-24	10	0.3996	2.365	326.9	3.126	0.588	2.930	0.138	0.0088	
		14	0.5444					1.984	0.137	0.0090	
		18	0.6953					1.137	0.134	0.0075	
		20	0.7673					0.997	0.134	0.0059	
		23	0.8753					0.474	0.134	0.0059	
	25-32		/	3.025	2.9 E6	8.174	0.227	/	/	/	
				a_1	b_1	c_1	d_1	a_2	b_2	c_2	d_2
	34-41		/	1.483	9129.1	6.52	0.454	0.298	0.260	3.95	0.529

6. Comparison of generalized force spectra

After modal decomposition, the physical motion equations can be de-coupled as

$$\ddot{q}_j(t)+2\xi_j\omega_j\dot{q}_j(t)+\omega_j^2 q_j(t) = F_j(t) \quad (j=1,\cdots,3n) \tag{11}$$

where $F_j(t)$ is the j^{th} generalized wind load. It can be calculated as follows

$$F_j(t) = \boldsymbol{\varphi}_j^{\mathrm{T}} \boldsymbol{R}\boldsymbol{p}(t) \Big/ M_j^* \tag{12}$$

where $\boldsymbol{\varphi}_j^{\mathrm{T}}$ is the j^{th} mode; $\boldsymbol{R}$ is the determination matrix for transforming the wind loads measured from the model at different levels of altitude to those on the real building floors; $\boldsymbol{p}(t)$ is the wind load vector at a measuring level; M_j^* is the j^{th} generalized mass.

So the j^{th} generalized force power spectrum is

$$S_{F_jF_j}(f) = \boldsymbol{\varphi}_j^{\mathrm{T}} \boldsymbol{R}\boldsymbol{S}_{pp}(f)\boldsymbol{R}^{\mathrm{T}}\boldsymbol{\varphi}_j \Big/ \left(M_j^*\right)^2 \tag{13}$$

where $\boldsymbol{S}_{pp}(f)$ is the power spectrum of $\boldsymbol{p}(t)$.

In order to verify the validity of the proposed mathematical models of wind force spectra on the 492 m height high-rise building, the first three order generalized force power spectra (the first three order modes are shown in Fig. 16) by formulae (ignoring the relevance of wind loads, that is, letting all the non-diagonal elements of $\boldsymbol{S}_{pp}(f)$ be zero) are compared to that by experiment, see Fig. 17. The comparison shows good agreement.

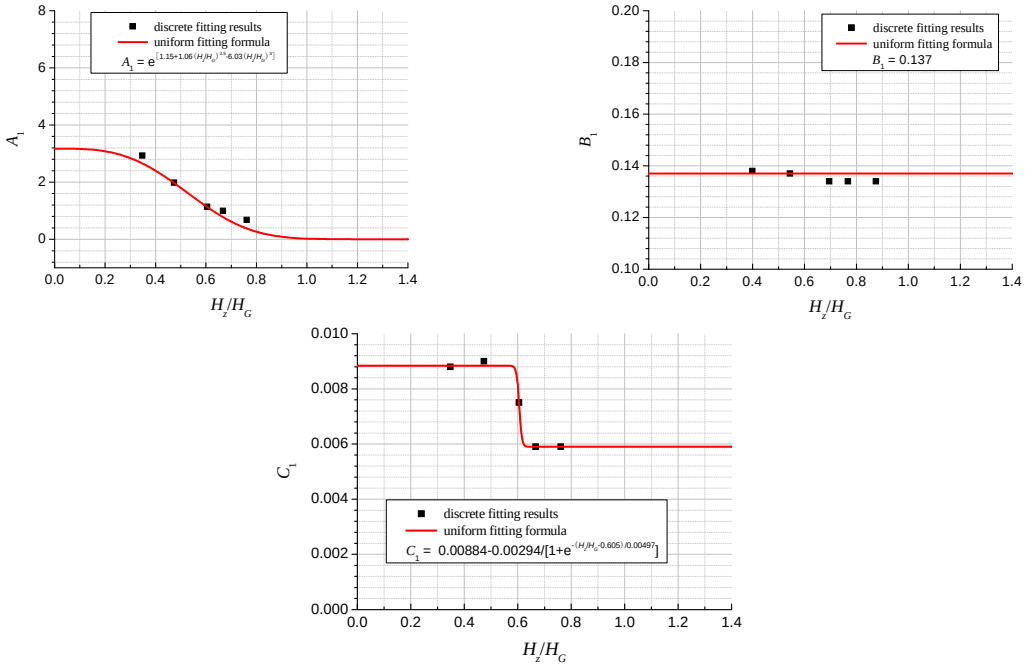

Fig. 15 Fitting results about the fitted parameters of the wind force spectrum peaks of RZ-axis at measurement levels of 8-24in wind direction of 315°

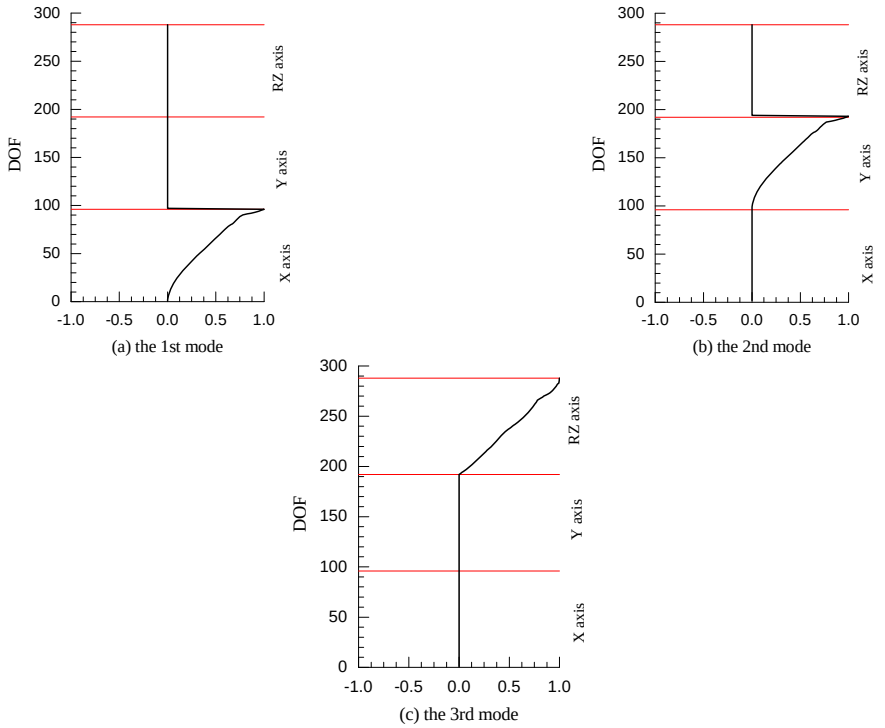

(a) the 1st mode (b) the 2nd mode

(c) the 3rd mode

Fig. 16 structural modes

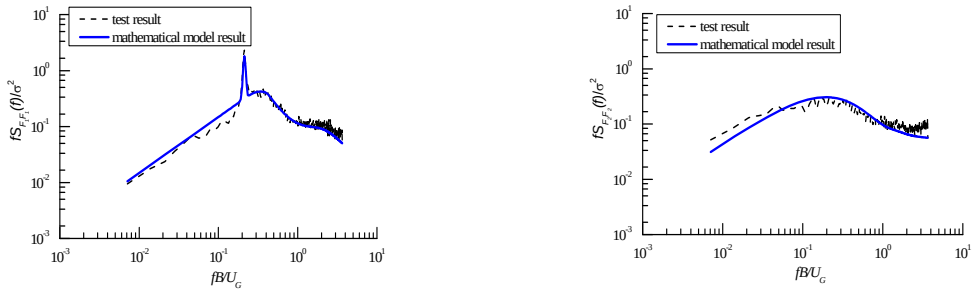

(a) The 1st generalized force spectrum (b) The 2nd generalized force spectrum

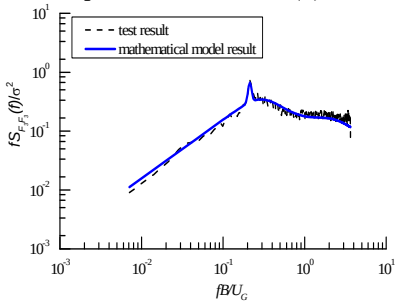

(c) The 3rd generalized force spectrum

Fig. 17 Comparisons of the first three generalized wind force spectra between the proposed mathematical models and the test results

7. Conclusions

Based on the investigation of characteristics (mainly in 315º, 0º and 45º wind direction)and mathematical expressions (in 315º wind direction)of power spectra of wind forces on a complex shaped super-tall building with a section varying along height, some conclusions can be drawn by taking the results in wind direction of 315º as example:

(1) The standardized power spectra of wind force coefficients at different levels of altitude have the following characteristics: in X axis (cross-wind) direction with height increasing, power spectra become flat and their basic frequency increase, peak value decrease, frequency band broaden, energy in high-frequency increase; in Y axis (along-wind) direction, power spectra are more flat and similar to wind spectrum, moreover, at the top part, energy in high-frequency increase; around Z axis (torsion)direction, the features of wind force power spectra along height are similar to that of X axis direction.

(2) The mathematical expressions of wind force spectra of the main structure in across-wind and torsional directions can be constructed by superimposition of an modified wind spectrum function and a peak function caused by turbulent flow and vortex shedding, respectively, while that in along-wind direction can only be constructed by the former, similar to wind spectrum. The proposed formulae well accord with test results.

(3) For such a high-rise building with complex shape but sections changing regularly along height, the fitting parameters of wind force spectra at different levels of altitude have some regular patterns. Therefore, they can be summarized with formulae or unification values, which will be convenient to set up the diagonal elements of wind load power spectral matrix for this high-rise building. The comparison of the first three order generalized force spectra shows that the proposed mathematical models of wind force spectra well accord with the experimental results.

Acknowledgments

The work described in this paper was supported by the National Natural Science Foundation (51208524), the Hunan Province Natural Science Foundation (12JJ4055), the Shanghai Education Committee Dawn Plan (04SG23), the Free Exploration Program of Central South University (201012200035), the China Postdoctoral Science Foundation (20100471227), and the Postdoctoral Science Foundation of Central South University. Any opinions and concluding remarks presented here are entirely those of the authors.

References

Architectural Institute of Japan (1996), AIJ *Recommendations for Loads on Buildings*.

Cheng, C.M. and Kareem, A. (1992), "Acrosswind response of reinforced concrete chimneys" *J. Wind Eng. Ind. Aerod.*, **43**, 2141-2152

Davenport, A.G. (1961), "The application of statistical concepts to the wind loading of structures", *Proc. Inst. Civ. Eng. London*, **19**, 449-472.

Davenport, A.G. (1967), "Gust loading factors", *J. Struct. Div. ASCE*, **93**, 11-34.

Gu, M. and Quan, Y. (2004), "Across-wind loads of typical tall buildings", *J. Wind Eng. Ind. Aerod*., **92**(13), 1147-1165.

Holmes, J.D. and Lewis, R.E. (1987), "Optimization of dynamics-pressure-measurement systems I. &II", *J.*

Wind Eng. Ind. Aerod., **25**, 249-290.
Irwin, H.P.A.H., Cooper, K.R. and Girard, R. (1979), "Correction of distortion effects caused by tubing systems in measurements of fluctuating pressures", *J. Wind Eng. Ind. Aerod.*, **5**(1-2), 93-107.
Islam, M.S., Ellingwood, and Corotis, R.B. (1990), "Transfer function models for determining dynamic wind loads on buildings" , *J. Wind Eng. Ind. Aerod.*, **36**(10), 449-458
Islam M.S., Ellingwood, and Corotis R.B. (1992), "Wind-Induced response of structurally asymmetric high-rise buildings", *J. Struct. Eng.- ASCE*, **118**(1), 207-222.
Kareem, A. (1982a), "Acrosswind response of buildings", *J. Struct. Eng. - ASCE*, **108**(4), 869-887.
Kareem, A. (1982b), "Fluctuating wind loads on buildings", *J. Eng. Mech. - ASCE*, **108**(6), 1086-1102.
Kareem, A. (1992), "Dynamic response of high-rise buildings to stochastic wind loads", *J. Wind Eng. Ind. Aerod.*, **42**(1-3),1101-1115.
Kwok, K.C.S. (1982), "Cross-wind response of tall buildings", *Eng. Struct.*, **4**(10), 256-262.
Kwok, K.C.S. (1995), "Aerodynamics of tall buildings", *Proceedings of the State of the art volume.9 ICWE*, New Delhi, India.
Liang, S.G., Liu, S.C., Li, Q.S., Zhang, L.L. and Gu, M. (2002), "Mathematical model of acrosswind dynamic loads on rectangular tall buildings", *J. Wind Eng. Ind. Aerod.*, **90(**12-15), 1757-1770.
Liang, S.G., Li, Q.S., Liu, S.C., Zhang, L.L. and Gu, M. (2004), "Torsional dynamic wind loads on rectangular tall buildings", *Eng. Struct.*, **26**(1), 129-137.
Lin, N. Letchford, C. Tamura, Y., Liang, B. and Nakamura, O. (2005), "Characteristics of wind forces acting on tall buildings", *J. Wind Eng. Ind. Aerod.*, **93**(3), 217-242.
Marukawa, H., Ohkuma, T. and Momomura, Y. (1992), "Acrosswind and torsional acceleration of prismatic high rise buildings", *J. Wind Eng. Ind. Aerod.*, **42**(1-3), 1139-1150.
Ministry of Construction P.R. China (2006), *Load code for the design of building structures - GB 50009 - 2006*, Chinese building industry press, Beijing, (in Chinese).
Saunders, J.W. and Melbourne, W.H. (1975), "Tall rectangular building response to cross-wind excitation". *Proceedings of the 4th Int. Conf. On Wind Effects on Buildings and Structures*, Cambridge University Press, Cambridge.
Simiu, E. and Scanlan, R. (1986), *Wind effects on structures: an introduction to wind engineering*, New York, Wiley Press.
Yeh, H. and Wakahara, T. (1992),"Wind-induced forces on a slender rectangular-column structure", *Proceedings of the 2EACWE*, Genova, Italy.
Zhou, Y., Gu, M. and Xiang, H.F. (1999a), "Alongwind static equivalent wind loads and responses of tall *buildings*. Part I: Unfavorable distributions of static equivalent wind loads", *J. Wind Eng. Ind. Aerod.*, **79**(1-2), 135-150
Zhou, Y., Gu, M. and Xiang, H.F. (1999b), "Alongwind static equivalent wind loads and responses of tall buildings. Part II: Effects of mode shapes", *J. Wind Eng. Ind. Aerod*., **79**(1-2), 151-158.

CC